

Magnetic Field Generation in High-Intensity-Laser-Matter Interactions

R. J. Mason¹ and M. Tabak²

¹*Los Alamos National Laboratory, Los Alamos, New Mexico 87545*

²*Lawrence Livermore National Laboratory, Livermore, California 94550*

(Received 3 June 1997)

A multifluid implicit plasma simulation code has been used to study the transport of hot electrons generated by an intense ($\geq 3 \times 10^{18}$ W/cm²) short-pulse 1.06 μ m laser into plasma targets over a broad range of densities $[(0.35-200)n_{\text{crit}}]$, as arising in the Fast Ignitor approach to inertial confinement fusion. The most intense (16–250 MG) magnetic fields generated in this interaction are traced to the ponderomotive push on background electrons, and tardy electron shielding. These fields can focus the heated electrons toward the axis of the beam, while impeding the direct return flow of background electrons. [S0031-9007(97)04996-X]

PACS numbers: 52.40.Nk, 52.35.Mw, 52.50.Jm, 52.65.Kj

The Fast Ignitor is an alternate approach to inertial confinement fusion (ICF) [1]. The concept employs conventional lasers to (1) compress a pellet of DT fuel to approximately 300 g/cm³. (2) Then, a several hundred picosecond laser is used to bore a hole with ponderomotive pressure through any low density atmosphere surrounding the compressed fuel. (3) Finally, a 3 to 50 ps 1.06 μ m laser is used to propagate energy to the DT surface, where it is absorbed, generating suprathermal electrons, which must deposit 3 to 60 kJ over an alpha particle range, raising the local temperature to 10 keV. This leads to ignition at the DT pellet surface. The full pellet then ignites by propagating burn [2]. As little as 100 kJ may be needed for the compression phase [1]. The hole boring can be accomplished with a 10^{17} – 10^{19} W/cm² pulse rising linearly as higher densities up to 100 times critical are encountered. An intensity of $\sim 10^{20}$ W/cm² is needed for the final short pulse, generating 1–5 MeV suprathermals.

Exploring parts of this scheme with particle-in-cell (PIC) codes, researchers have reported significant light absorption, target surface deformation in mildly overdense plasmas ($4n_{\text{crit}}$) [3,4], and the forging of open channels in underdense ($<0.5n_{\text{crit}}$) plasmas [5]. They have predicted the occurrence of intense (~ 100 MG) magnetic fields in both regimes. In this Letter, we have used the multifluid implicit ANTHEM [6,7] model to provide the first high-intensity simulations for a broad range of densities $[(0.35-200)n_{\text{crit}}]$ appropriate to the Fast Ignitor. ANTHEM can venture into density and collisional regimes that are inaccessible to PIC codes. We establish that the most intense fields (16 to 250 MG) seen in these interactions can arise from the push given to the background electrons by the ponderomotive force (PMF) of the incident laser beam, and the tardy development of electron shielding currents. This is consistent with the mechanisms proposed by Sudan [8], and Tripathi and Liu [9]. These fields can funnel the laser generated hot electrons into a narrow channel along the axis of the spot, while impeding the direct return flow of cold background electrons.

For the present study ANTHEM was configured to model target plasmas consisting of fluid ions and cold background fluid electrons. Laser deposition converted a portion of the cold electrons into an additional hot electron fluid. Inertia was retained for both electron components. The electromagnetic fields were obtained from the full Maxwell's equations implicitly. The hot electrons were slowed by drag against the cold background electrons. Both electron components were scattered against the ions at the classical rate. A comprehensive description of ANTHEM for ICF applications is given in [6,7] and [10–12], with alternate applications in [13]. ANTHEM was augmented for high laser intensities by time-advancing equations for hot and cold relativistic electron momenta $\mathbf{p}_{h,c}$, and moving the electrons with velocities $\mathbf{v} = \mathbf{p}/\gamma$, in which γ is the Lorentz factor. We also introduced a ponderomotive force [14] that separately accelerated the two electron fluid components, $\mathbf{F}_{h,c} = -(\omega_{p,h,c}^2/2\omega^2)\nabla I \sim n_{h,c}\nabla I$, in which I is the laser intensity, and $\omega_p^2 = 4\pi e^2 n/m_0\gamma$, where m_0 is the electron rest mass.

We used a Cartesian mesh with 50×50 cells. Light at 1.06 μ m was input from the right with a simple grid following algorithm. Reflected light passed back along the same grid lines until it left the problem. Our pulse had a Gaussian spatial envelope with a 3 μ m full width at half maximum. It rose linearly over a 41 fs interval to peak intensity and held constant thereafter. We included inverse-bremsstrahlung, acting everywhere along the light path, and “dump-all” deposition at the critical surface. The deposition locally depletes the cold electron fluid, and correspondingly creates enough hot electron fluid at zero drift velocity to account for the absorbed energy. Acting under their static pressure, the hot electrons spread inwards and draw a cold electron return current. The hot electrons also spread outwards toward the laser, filling the corona within a local Debye length of the ions, possibly driving fast ion blowoff [15]. The hot electron temperature T_h and the fractional dump-all f_d at critical were set by previous PIC code experience, i.e., Fig. 3

of Wilks *et al.* [3]. Mirror boundary conditions were imposed vertically. The hot electron fluid was absorbed near the back boundary, with the exiting electrons added to the returning cold electron fluid.

First, we simulated the interaction of a drive beam at peak intensity $I_d = 3.3 \times 10^{18}$ W/cm² with a 4×10^{21} cm⁻³ density hydrogen plasma. We assumed 30% absorption, so that the maximal total intensity (incident plus reflected) was $I = 5.6 \times 10^{18}$ W/cm². The hot electron emission temperature was set at $T_{he} = 700$ keV. The cold background temperature T_c was set at 4 keV to match [3]. However, similar results were obtained for initial background temperatures as low as $T_c = 1$ eV. Figure 1 shows that the critical surface was pushed 1.9 μ m into the plasma by 340 fs. This agrees well with the Ref. [3] plasma velocity determination from $nM_p u^2 = I/c$, where M_p is the proton mass and u is the penetration speed. We also see an overdense magnetic field, corresponding to the injection of electron flux into the target. However, we calculate a lower peak magnetic intensity, i.e., only 16 MG. This matches $|B| \leq 4\pi en_{h-max} c \Delta x$, with $\Delta x \approx 0.1 \mu$ m determined from the gradient scale our Fig. 1 magnetic contours. We calculate a maximum hot emitted density, $n_{h-max} = 1.3 \times 10^{21}$ cm⁻³ near critical. Outside in the target corona, we observe a conventional thermoelectric field [16] (peaking at ~ 22 MG) from electrons flowing out toward the laser. The maximum overdense field increases to 37 MG when I_d is doubled to 6.6×10^{18} W/cm², and to 85 MG at 240 fs when I_d is quadrupled.

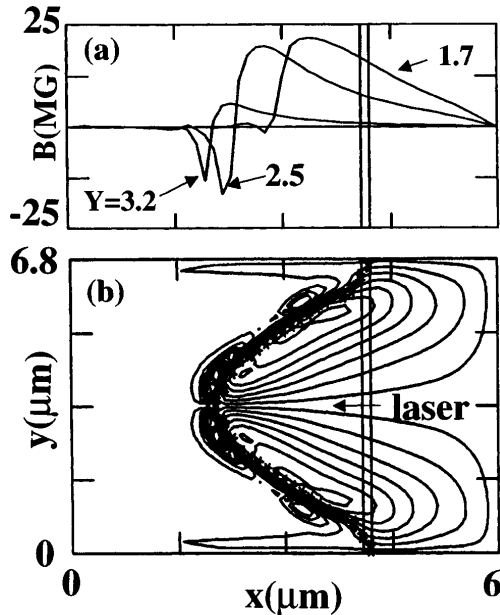


FIG. 1. In a $4n_{crit}$ plasma at 340 fs: (a) The magnetic field profiles along axial cuts at vertical positions $y = 1.7, 2.5,$ and 3.2μ m, all below the center line, under a total laser intensity (i.e., drive + reflected) of $I = 5.6 \times 10^{18}$ W/cm², (b) corresponding 2D contours calibrated by the curves in (a). The left vertical fiducial marks the initial location of the plasma edge; right marks the vacuum. Stars mark the instantaneous critical surface.

In another simulation for the same $T_h, f_d,$ and drive intensity, but with a denser $10n_{crit}$ target, we have observed a larger internal B field (~ 45 MG), and a peak hot electron density of $\sim 1.1 \times 10^{21}$ cm⁻³. The incident hot electron stream tends to focus on axis. At $50n_{crit}$ (corresponding roughly to solid density DT fuel) and the same laser intensity, we find that the peak magnetic field increased to ~ 80 MG. When at this density the drive is increased to 1.3×10^{19} W/cm² with $T_h = 1$ MeV and $f_d = 0.5$, the overdense B -field maximum rises to 180 MG at 340 fs, and the maximum hot electron density increases to 2.5×10^{21} cm⁻³. We show this in Fig. 2, along with the incident, return, and total electron fluxes. The incident hot electron stream is now strongly focused on the axis of the beam with additional flux running in along the boundaries; in these locations both the PMF and B field are weakest. The return current is also largely axial. The net electron flux flows into the target at its center and out at the edges, in agreement with Sudan's Fig. 1 [8]. Our Fig. 2(c) shows that the hot electron density peaks near the critical surface. The PMF appears to present a barrier to direct return of the cold electrons. At higher background densities, the cold electron flux $n_c \mathbf{v}_c$ needed to cancel the hot emission returns at a lower velocity $\mathbf{v}_c = n_h \mathbf{v}_h / n_c$, increasing the effectiveness of the repulsive ponderomotive barrier. In the absence of a return flow, the direct hot electron penetration is impeded. Also, we see that a strong shock (4/1 density jump) has moved 3 μ m into the background plasma. In the calculation for Fig. 2, the B field reaches a peak value of 250 MG at 200 fs, and then declines to 103 MG by 450 fs. In a similar run, in which the laser drive was shut down at 200 fs, the fields manifested a "frozen in" nature—unlike the Sudan prediction—such that they were actually more intense, i.e., 160 MG at 450 fs. The hot electron density is, however, down by a factor of 40 from the constant intensity case at this time, since no new suprathermals are being generated. At a still higher density of 2×10^{23} cm⁻³, which corresponds to singly shocked solid DT, we still measure a 225 MG B field at 290 fs; see Figs. 3(a) and 3(b). However, the peak B -field region (and bored hole) is half the Fig. 2 width, and electron trapping is reduced as the electrons pass around the central peak field region and into the target.

Classical resistivity was included in all of our runs. It has no notable effect at DT densities of $50n_{crit}$ and below, even with the initial plasma temperature started at 1 eV. This is because the cold electrons undergo joule heating and stagnation heating at near critical to 60 keV by 130 fs. Their high thermal conductivity then spreads this high temperature and corresponding low resistivity back through the background plasma. Our $200n_{crit}$ simulation was started at 0.1 keV, corresponding to compressive or radiative preheating of the fuel, in order to avoid additional electrostatic inhibition of the suprathermals, as recently analyzed by Bell *et al.* [17] for higher Z solids.

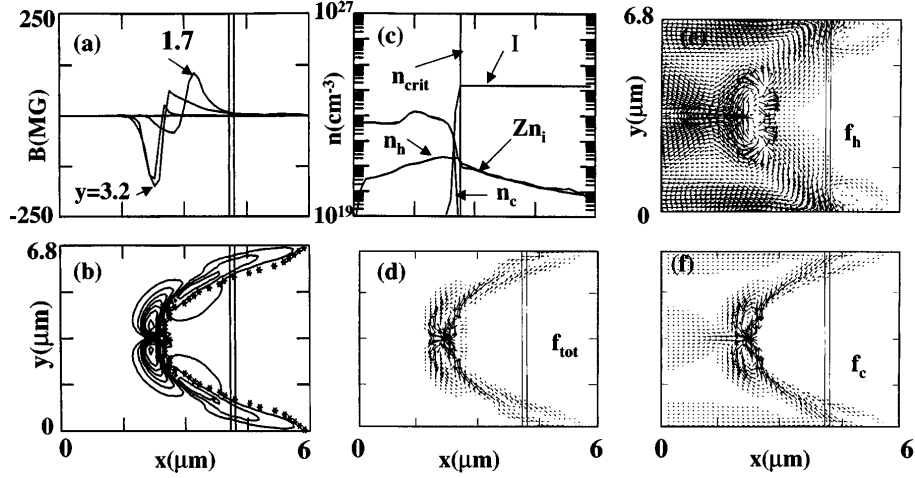


FIG. 2. At $10n_{\text{crit}}$, $I_d = 1.3 \times 10^{19}$ W/cm² and 340 fs: (a) axial B -field cuts, (b) corresponding magnetic contours, (c) the hot n_h , and cold n_c electron densities, Z times the ion density n_i in cm⁻³, and the total laser intensity I (relative units), (d) the total flux f_{tot} of hot and cold electrons, (e) the incident hot flux $f_h = n_h \mathbf{v}_h$, and (f) the returning cold flux $f_c = n_c \mathbf{v}_c$.

In all of our cases, the B field reverts to the thermoelectric [16] polarity and resides only in the subcritical corona if the ponderomotive force is set to zero; see Figs. 3(c) and 3(d). Retention of the PMF on just the hot electrons has the same effect; i.e., we see no supercritical magnetic field, but we do see a reduced hot electron density near the surface. The background cold electrons have the steepest density gradient, and crucially contribute to the field generation. For constant total I , we find that both the hole boring rate and overdense field are largely insensitive to changes in the absorption fraction. In fact, the same results are obtained when there is no absorption, no hot electron emission, and no hot streaming into the target— but only the push from the PMF.

Tripathi and Liu [9] have indicated that near the target surface, and in the laser deposition channel in front of it, the ponderomotive force of a short pulse gives the individual electrons a velocity $\mathbf{v} \sim \nabla I$, so that the net electron current is $\mathbf{j} = -nev \sim n\nabla I$. Since $\nabla \times \mathbf{j} \neq 0$, from Maxwell's equations they predict the development of a ponderomotively driven quasistatic B field, i.e., $c^2 \nabla^2 \mathbf{B} = \nabla \times [an\nabla I + \dots]$; where α is a constant. Let

us see how this field is manifest in our calculations. In the nonrelativistic limit, the cold electrons are advanced with a momentum equation

$$\mathbf{f}^{(m+1)} = \mathbf{f}^{(m)} - \frac{\nabla \cdot \mathbf{P}}{m} \Delta t - \frac{\omega_p^2}{2mc\omega^2} \nabla I \Delta t - \frac{ne}{m} \left(\mathbf{E}^{(m+1)} + \frac{\mathbf{v}^{(m+1)} \times \mathbf{B}^{(m)}}{c} \right) \Delta t, \quad (1)$$

in which $\mathbf{f} = n\mathbf{v}$ is the electron flux, and $\nabla \cdot \mathbf{P}$ includes both the dynamic and static electron pressures. For heuristics, in this discussion we neglect the ion motion, and the electron-ion collisions, although these effects are included in the full calculations. Also, for simplicity, we consider the motion of just a single cold electron component, employ fully forward numerical time centering, and leave $\mathbf{v}^{(m+1)}$ explicitly represented although it is determined implicitly in terms of the $\mathbf{v}^{(m)}$ in the code. Then, in accordance with Ampere's law, during each computational cycle the electric field advances as $\mathbf{E}^{(m+1)} = \mathbf{E}^{(m)} - (4\pi e \mathbf{f}^{(m+1)} - c\nabla \times \mathbf{B}^{(m+1)}) \Delta t$. This rearranges to

$$\mathbf{E}^{(m+1)} = \frac{\mathbf{E}^{(m)} - [4\pi e \mathbf{f}^{(m)} - c\nabla \times \mathbf{B}^{(m+1)}] \Delta t + \left[\frac{-\nabla \cdot \mathbf{P}}{en} - \frac{\mathbf{v}^{(m+1)} \times \mathbf{B}^{(m)}}{c} - \frac{4\pi e}{2mc\omega^2} \nabla I \right] (\omega_p \Delta t)^2}{1 + (\omega_p \Delta t)^2}, \quad (2)$$

as presented in [6,7] without the ponderomotive term. The new magnetic field for each cycle is then found by coupling this to Faraday's law, $\mathbf{B}^{(m+1)} = \mathbf{B}^{(m)} - c\nabla \times \mathbf{E}^{(m+1)} \Delta t$.

In colder plasmas with low intensity laser illumination, we can often ignore the dynamic pressure terms, leaving just the scalar pressure $\nabla \cdot \mathbf{P} = \nabla n \kappa T$. We can also ignore initial currents and fields. If we assume cold electrons so that the time step can be large, we can move the electrons across many skin depths in a time step, i.e., $\Delta x = v\Delta t \gg c/\omega_p$, so $\omega_p \Delta t \gg c/v \gg 1$.

Then, since the remaining coefficients of the ponderomotive ∇I are constants, (2) combines with Faraday's law leaving mainly the traditional thermoelectric magnetic field, $\mathbf{B}^{(m+1)} \sim \nabla n \times \nabla T$. Alternatively, at high Fast Ignitor intensities, the electrons are accelerated to nearly the speed of light. In our dense plasma simulations, the typical cell size is less than $0.1 \mu\text{m}$ (to resolve the skin depth), and at least three time steps are needed for accurate calculations as electrons cross a cell, so $\Delta t \leq 1.1 \times 10^{-16}$ s. Above critical at 10^{22} cm⁻³ densities $\omega_p = 5.6 \times 10^{15}$ s⁻¹, giving $(\omega_p \Delta t)^2 \leq 0.4$. In such

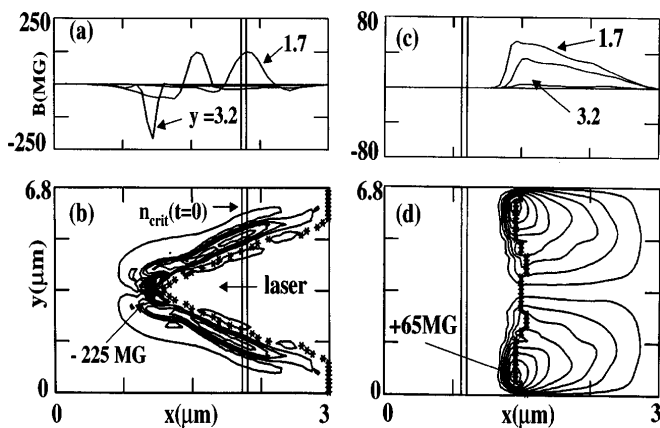


FIG. 3. Magnetic field: (a) Cuts and (b) contours at 290 fs in a $200n_{\text{crit}}$ plasma exposed to an incident $I_d = 1.3 \times 10^{19}$ W/cm² laser with 50% absorption into hot electrons at $T_h = 1$ MeV; (c),(d) corresponding results at 340 fs with PMF “off”—for the plasma initially shifted left to allow room for the blowoff.

cases, the background electrons respond too slowly to shield against the PMF driven charge separation electric field, which in (2) retains a variation $\sim n\nabla I$, so the magnetic field can evolve a component $\mathbf{B} \sim \nabla n \times \nabla I$, accounting for the calculated results. This is in strong contrast to (and may be complemented by) alternate mechanisms for magnetic field production derived from instability, such as Weibel [18], of the net distribution function of hot streaming [19], and cold background electrons.

With our usual Gaussian envelope, the electrons are given the hardest push on the axis. This sets the B -field polarity corresponding to electron flow away from the laser and into the target center. However, with a spatially flat-topped pulse, we found that the surface B field vanishes, except for small disturbances at the pulse edges. When a cooky cutter (more intense at the edges than the center) beam is employed, the overdense B -field polarity reverses, corresponding to a central electron stream toward the laser.

Alternatively, looking at lower density interactions appropriate to energy channeling in the Fast Ignitor, we found that (1) for low supercritical densities, i.e., $n_e \leq 1.6 \times 10^{21}$ cm⁻³ and $I_d = 3.3 \times 10^{18}$ W/cm², the central one micron portion of the beam just burns through the target, due to the relativistic lowering of the plasma frequency as electrons are heated. A doubling of the drive intensity I_d doubles the initial burnthrough width, and leads to significant beam pinching over $2 \mu\text{m}$ of depth by 50 fs. (2) Calculations, as in [5] of the interaction of a 10^{19} W/cm² $1.06 \mu\text{m}$ Gaussian beam with a $0.35n_{\text{crit}}$ plasma, and employing the anomalous absorption of 40% of the light into 1 MeV hot electrons over a $40 \mu\text{m}$ length, show channel formation over 440 fs with the central channel density dropping to $0.2n_{\text{crit}}$. Hot electrons leave the

center laterally [20], setting up an electric field to hold back charge for quasineutrality. This pushes ions to the side. With the PMF included, we observe a ~ 10 MG magnetic field looping around the density maxima created at the channel edge. The magnetic polarity corresponds to electrons following the laser photons. Such fields were anticipated in [9]. When the PMF is turned off in simulation, the ion expulsion dynamics continues, but the magnetic field is negligible.

If refraction were added to our light transport algorithm, this would focus the light into the lower density regions of a channel or PMF-indented target, raising the central laser intensity, as seen in [5], and boring a deeper central hole in both the corona and the target.

We are grateful to R. Sudan, J. Meyer-ter-Vehn, O. Willi, J. Cobble, M. Cray, and M. Campbell for helpful discussions and encouragement. This work was supported by the U.S. DOE.

- [1] M. Tabak, J. Hammer, M. E. Glinsky, W. L. Kruer, S. C. Wilks, J. Woodworth, E. M. Campbell, M. D. Perry, and R. J. Mason, *Phys. Plasmas* **1**, 1626 (1994).
- [2] G. S. Fraley, E. J. Linnebur, R. J. Mason, and R. L. Morse, *Phys. Fluids* **17**, 474 (1974).
- [3] S. C. Wilks, W. L. Kruer, M. Tabak, and A. B. Langdon, *Phys. Rev. Lett.* **69**, 1383 (1992).
- [4] M. F. Ivanov, A. V. Ivlev, and M. G. Keidjan, *Plasma Phys. Rep.* **22**, 124 (1996).
- [5] A. Pukhov and J. Meyer-ter-Vehn, *Phys. Rev. Lett.* **76**, 3975 (1996); M. Borghesi *et al.*, *Phys. Rev. Lett.* **78**, 879 (1997).
- [6] R. J. Mason, *J. Comput. Phys.* **71**, 429 (1987).
- [7] R. J. Mason and C. W. Cranfill, *IEEE Trans. Plasma Sci.* **14**, 715 (1986).
- [8] R. N. Sudan, *Phys. Rev. Lett.* **70**, 3075 (1993).
- [9] V. K. Tripathi and C. S. Liu, *Phys. Plasmas* **1**, 990 (1994).
- [10] R. J. Mason, in *Multiple Time Scales*, edited by J. Brackbill and B. I. Cohen (Academic Press, New York, 1985), p. 233.
- [11] R. J. Mason, *J. Comput. Phys.* **51**, 484 (1983).
- [12] R. J. Mason, P. L. Auer, R. N. Sudan, B. V. Oliver, C. E. Seyler, and J. B. Greenly, *Phys. Fluids B* **5**, 1115 (1993).
- [13] R. J. Mason, *IEEE Trans. Plasma Sci.* **23**, 465 (1995).
- [14] F. F. Chen, *Introduction to Plasma Physics and Controlled Fusion* (Plenum Press, New York, 1984), 2nd ed., p. 307.
- [15] A. R. Bell *et al.*, *Phys. Rev. E* **48**, 2087 (1993).
- [16] J. A. Stamper, K. Papadopoulos, R. N. Sudan, S. O. Dean, E. A. McClean, and J. M. Dawson, *Phys. Rev. Lett.* **26**, 1012 (1971).
- [17] A. R. Bell, J. R. Davis, and S. Guerin, *Plasma Phys. Control. Fusion* **39**, 653 (1997).
- [18] E. W. Weibel, *Phys. Rev. Lett.* **2**, 83 (1959).
- [19] A. Pukhov and J. Meyer-ter-Vehn, *Bull. Am. Phys. Soc.* **41**, 1502 (1996).
- [20] J. A. Cobble, R. P. Johnson, and R. J. Mason, *Phys. Plasmas* **4**, 3006 (1997).